LETTER • OPEN ACCESS

Probing room temperature indirect and minimum direct band gaps of h-BN

OPEN ACCESS

Applied Physics Express 17, 091001 (2024) LETTER

https://doi.org/10.35848/1882-0786/ad777a

Probing room temperature indirect and minimum direct band gaps of h-BN

N. K. Hossain, A. Tingsuwatit, Z. Alemoush, M. Almohammad, J. Li, J. Y. Lin, and H. X. Jiang*

Department of Electrical and Computer Engineering, Texas Tech University, Lubbock, TX 79409, United States of America

*E-mail: hx.jiang@ttu.edu

Received August 28, 2024; revised September 2, 2024; accepted September 4, 2024; published online September 19, 2024

Hexagonal boron nitride (h-BN) has attracted considerable interest as an ultrawide bandgap (UWBG) semiconductor. Experimental studies focused on the detailed near band-edge structure of h-BN at room temperature are still lacking. We report a direct experimental measurement of the near band-edge structure performed on h-BN quasi-bulk wafers via photocurrent excitation spectroscopy (PES). PES resolved the band-to-band transitions near M- and K-points in the Brillion zone (BZ), from which the room temperature indirect band gap of E_g^{MK} ~6.02 eV, minimum direct bandgap at M-point of $E_g^M = 6.36$ eV and next lowest direct energy bandgap at K-point of $E_g^K = 6.56$ eV, have been simultaneously determined for the first time experimentally. The measured energy differences between K- and M-points in the conduction band minimum (CBM) and valence band maximum (VBM) are $\Delta E_C^{MK} = 0.54$ eV and $\Delta E_V^{MK} = 0.34$ eV, respectively, in good agreement with the calculation results. Significantly differing from its III-nitride wurtzite counterparts, in which only electrons and holes in the conduction and valence band extremes at the Γ-point are predominantly involved in the optical and transport processes, the results highlighted that charge carriers associated with both M- and K-valleys control to the optical excitation, recombination and charge transport processes in h-BN. © 2024 The Author(s). Published on behalf of The Japan Society of Applied Physics by IOP Publishing Ltd

The group III-nitride wide bandgap (WBG) semiconductors have contributed to the revolution of lighting, consumer electronics and power electronics[1–9] and are expected to make an impact in full spectrum solar energy conversion, sterilization, and UV curing technologies.[10–12] Due to its close lattice match to graphene and chemical inertness, hexagonal boron nitride (h-BN) in its 2D form has been intensively studied as a template, insulating and barrier material for the construction of 2D structures such as graphene based heterostructures[13] and single photon emitters.[14] As a semiconductor, h-BN possesses exceptional physical properties including an ultrawide bandgap (UWBG) of ~6 eV,[15–19] high breakdown field of ~12 MV cm^{-1},[20] high in-plane thermal conductivity of ~550 W/m·K[21] and large interaction cross-section between thermal neutrons and its atomic constituent ^{10}B of ~3840 Barns (=3.84 × 10^{-21} cm^2).[22,23] As such, h-BN is an attractive UWBG material for applications including deep-UV (DUV) emitters and detectors,[15–19,24–26] solid-state neutron detectors,[26–29] and potentially for power electronic devices.

Previous theoretical and experimental studies have revealed significant differences in the fundamental optical properties between h-BN[18,19,30–41] and wurtzite AlN[42–44] having a comparable energy bandgap. All wurtzite III-nitrides (AlN, GaN, and InN) have direct bandgaps with the conduction band minimum (CBM) and valence band maximum (VBM) located at the Γ-point.[42–44] Furthermore, energies at other high symmetry points in the Brillouin zone (BZ), such as L- and K-points in wurtzite III-nitrides, are much higher than those at the Γ-point. Consequently, the transport and optical properties of InN, GaN, and AlN, including the carrier effective masses and mobilities and band-edge optical transitions, are predominantly determined by the band parameters at the Γ-point. In contrast, in h-BN, the CBM and VBM are at M-and K-points in the BZ, respectively,[18,19,30,32,37] making h-BN an indirect bandgap material. The calculated energy differences between K- and M-points in the conduction and valence bands appear to be quite small,[18,37] which makes it very challenging to experimentally measure the room temperature indirect bandgap, as well as minimum direct energy bandgaps at the M- and K-points. Nevertheless, knowing the bandgaps at room temperature is important because most devices will perform at room temperature. Near band-edge optical transitions of high-quality h-BN bulk and epitaxial materials generally exhibit complicated phonon-assisted excitonic features at low temperatures which tend to disappear at room temperature.[19,31–40] On the other hand, room temperature photocurrent excitation spectroscopy measurements have been attempted previously, which did not yield a detailed band-edge structure but implied that direct excitation involving the lowest direct bandgaps is a dominant process.[41,45] Consequently, the experimental results concerning the detailed band structure describing the CBM and VBM at M- and K-points in the BZ in h-BN are still lacking. Additionally, the consequences of this complicated band structure on its potential applications have not been fully addressed and understood.

In this work, photocurrent excitation spectroscopy has been performed on h-BN quasi-bulk wafers to directly measure the band-to-band transitions involving K- and M-points in the BZ, with the aim to obtain an improved understanding of the detailed band-edge structure at room temperature and its consequences on the optical and transport processes in h-BN. In terms of practical device implementation, improved ability for producing large size quasi-bulk wafers (or thick epitaxial films) with high crystalline quality is vital for utilizing h-BN as an active host or substrate for a range of photonic and electronic device applications, as the more available millimeter sized bulk crystals produced by high pressure and high temperature (HPHT) and metal flux solution methods[16,17,20,21,46,47] are impractical to serve as substrates or for device implementation.

Hydride vapor-phase epitaxy (HVPE) growth technique was utilized to produce h-BN quasi-bulk wafers used here.[48,49] The greatest advantage of the HVPE method is its ability to provide higher growth rates of 10 s to 100 s μm/h compared to a growth rate that is limited to a few μm/h for the metal organic CVD (MOCVD) method. In the development of GaN, the HVPE method has been the default choice for attaining quasi-bulk crystals in large wafer sizes. Another

advantageous feature is that the precursors of the HVPE are carbon free, whereas carbon impurities tend to form undesired deep level impurities in h-BN.[50,51] Quasi-bulk wafers were synthesized at 1450 °C on 4"-diameter c-plane sapphire substrates. BCl_3 and NH_3 were employed as precursors for B and N, respectively.[48,49] The growth rate employed was around 15 μm h^{-1}. Thick h-BN tends to self-separate from the sapphire to form a freestanding wafer after growth during cooling down due to its layered crystalline structure. The thickness of the wafer used in this study is about 100 μm as probed by the profilometry measurement.

The X-ray diffraction (XRD) pattern in the 2θ-ω scan revealed that the h-BN (002) peak position (stacked planes in the c-direction) of these samples is centered at $2\theta = 26.72°$, corresponding to a c-lattice constant of nearly 6.66 Å.[49] A detailed comparison has been made previously among HPHT bulk crystals and HVPE quasi-bulk wafers.[49] The XRD full width at the half maximum (FWHM) of the h-BN (002) peak observed in a 100 μm thick quasi-bulk wafer was 0.29°, in comparison to a value of 0.14° observed in a HPHT bulk crystal.[46] To further verify the crystalline structure of the HVPE quasi-bulk wafers, a transmission electron microscope (TEM) measurement was employed here to directly reveal the spacing between the stacked planes in the c-direction. Figure 1(a) contains a portion of an expanded cross-sectional view of a TEM image of a quasi-bulk wafer, which demonstrates that these quasi-bulk wafers have an excellent layered crystalline structure with a spacing of 3.33 Å between the stacked layers in the c-direction.

Figure 1(b) shows the room temperature Raman spectrum. The observed mode at $\Delta\sigma = 1366\,cm^{-1}$ matches the value expected for the E_{2g} in-plane shear mode in bulk h-BN,[51] suggesting that the freestanding quasi-bulk wafer is nearly stress free. The observed Raman spectral linewidth is $16\,cm^{-1}$, which is narrower than a value of $25\,cm^{-1}$ reported previously for h-BN quasi-bulk wafers with a similar thickness[52] but is larger than a typical value of $8\,cm^{-1}$ observed in small bulk crystals grown by the HPHT method.[47] The results shown in Fig. 1 indicate that the HVPE quasi-bulk crystals used here have a pure h-phase (layered structure). However, the comparison results of the XRD and Raman measurements among the HPHT and HVPE crystals argue for a continued effort to further improve the structures both in the c-direction and in the c-plane for the HVPE grown quasi-bulk crystals.

Lateral detectors with a width of 1.5 mm were fabricated by depositing metal contacts of Ni/Au (20 nm/30 nm) on the two edges by e-beam evaporation, as illustrated in Fig. 2(a). Figure 2(b) is an optical image of a fabricated device for the PES measurements. A laser-driven light source (LDLS) covering a wavelength range between 190 and 2400 nm coupled with a triple grating monochromator was used as a variable wavelength excitation source. A Kiethley source-meter was used to supply the bias voltage and an electrometer was used to record the photocurrent.

A photoexcitation current spectrum of a quasi-bulk sample is shown in Fig. 2(c). Judging by the signal to noise ratio, we believe that four spectral peaks have been resolved near the band-edge at $E_1 = 5.93$ eV, $E_2 = 6.10$ eV, $E_3 = 6.36$ eV, and $E_4 = 6.56$ eV. The peak in a photocurrent excitation spectrum represents a direct photoexcitation of free carriers from either a band-to-band or impurity-to-band transition. With these peaks observed near or above ~6 eV, each peak can be attributed to the band-to-band transition type since the energy levels of common impurities/defects are all larger than 0.5 eV in h-BN.[50,51] The band structure calculation[18,32,37] and phonon-assisted photoluminescence (PL) measurement results[19,36–40] have provided us with the following insights concerning the structure of the band-edges of h-BN: (a) h-BN is an indirect gap semiconductor with a bandgap around 6 eV; (b) the CBM is at M-point and the VBM is at K-point, and (c) the slope of the dispersion of the M-K section in the conduction band is slightly larger than that in the valence band,[18,37] implying that the minimum direct energy bandgap of h-BN is at M-point. However, the room temperature indirect energy bandgap and the energy level differences

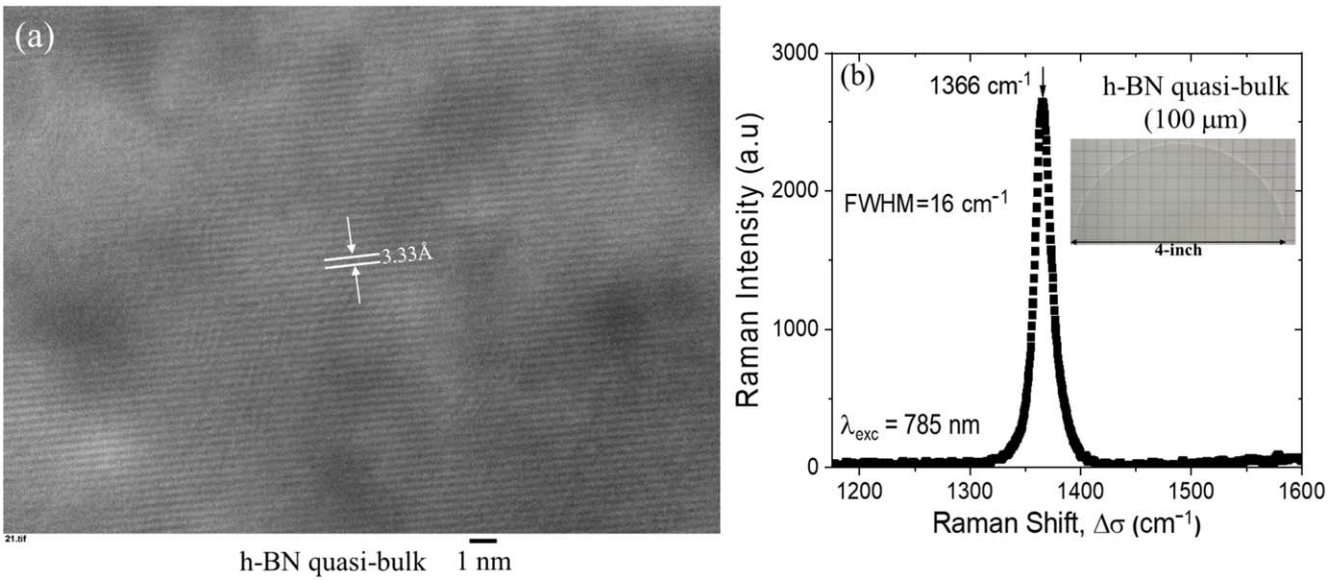

Fig. 1. (a) The cross-sectional view of TEM image of a freestanding h-BN sample, measuring a spacing of 3.33 Å between the stacked layers in the c-direction. (b) The room temperature Raman spectrum of a 100 μm thick h-BN quasi-bulk wafer produced by the HVPE. The inset shows a photo of a 4"-diameter freestanding h-BN quasi-bulk wafer.

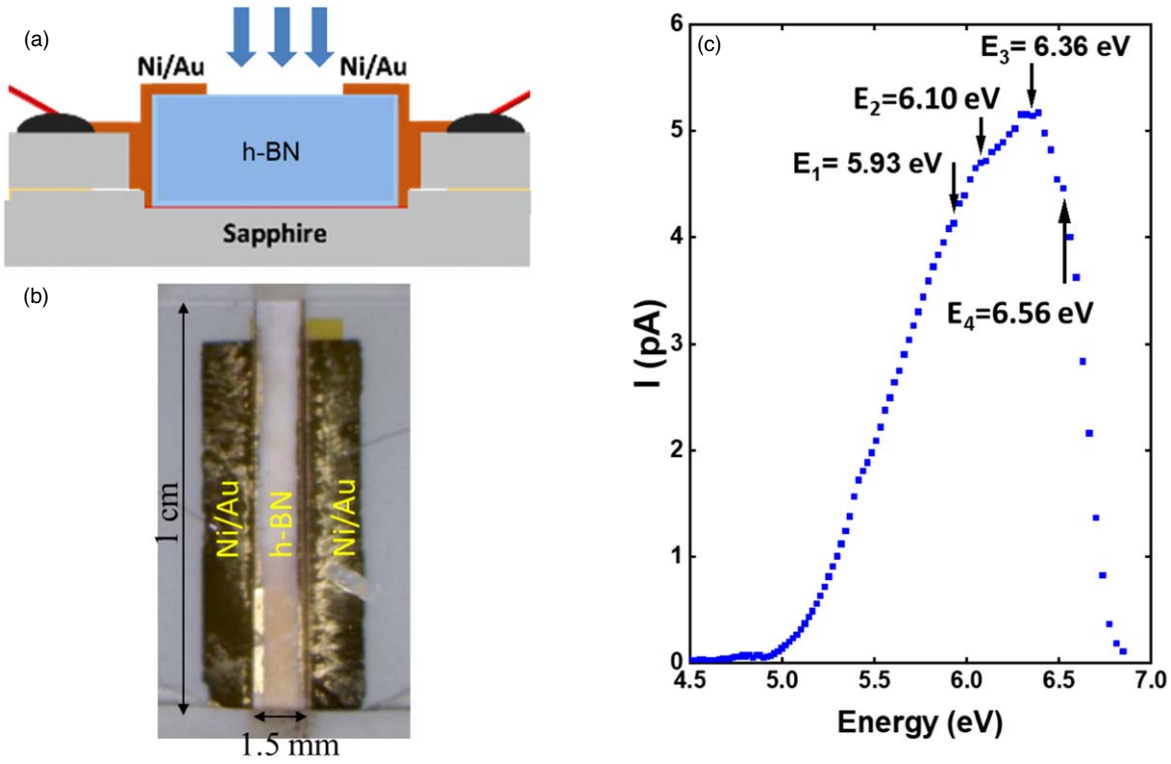

Fig. 2. (a) Schematic diagram and (b) photo of a fabricated h-BN lateral device used for photocurrent excitation spectroscopy (PES) measurements. (c) Photocurrent excitation spectrum of h-BN, resolving four peaks near the band-edge region at $E_1 = 5.93$ eV, $E_2 = 6.10$ eV, $E_3 = 6.36$ eV, and $E_4 = 6.56$ eV.

between CBM and VBM at M- and K-points have not been determined experimentally.

Due to the nature of its indirect bandgap, the participation of various phonons is necessary in optical emission processes to conserve the momentum and energy.[19,30,36–40] From the point view of momentum conservation, the involved phonon in such optical recombination processes must have the wave vector, $\boldsymbol{q}$, pointing from M-point to K-Point, $\boldsymbol{q}=\boldsymbol{MK}$.[19] In an optical recombination process in h-BN, a phonon can be emitted or absorbed. Based on this understanding, the peaks observed at $E_1 = 5.93$ eV and $E_2 = 6.10$ eV can be attributed to the optical excitation of electrons from K-point of the VBM to M-point of the CBM assisted by emitting and absorbing a phonon of wave vector $\boldsymbol{MK}$, we therefore have

$$E_1 = E_g^{MK} - E_p, \tag{1a}$$

$$E_2 = E_g^{MK} + E_p. \tag{1b}$$

In Eq. (1), E_g^{MK} is the energy of bandgap gap of h-BN, which is indirect with the CBM and VBM located at M-point and K-point, respectively, and E_p denotes the energy of the phonon assisted in the emission (−)/absorption (+) process. Equation (1) then provides,

$$E_g^{MK} = E_g = (E_2 + E_1)/2 = (6.10\ \text{eV} + 5.93\ \text{eV})/2 = 6.02\ \text{eV}, \tag{2a}$$

$$E_p = (E_2 - E_1)/2 = (6.10\ \text{eV} - 5.93\ \text{eV})/2 = 0.085\ \text{eV}. \tag{2b}$$

The obtained indirect bandgap of 6.02 eV (T = 300 K) agrees very well with a value of 6.08 eV at 10 K deduced from two-photon PL excitation spectroscopy measurements,[19] considering the fact that *Eg* tends to decrease with increasing temperature, which affirms our assignments of the observed four peaks near the band-edge in the photoexcitation spectrum shown in Fig. 2. To the best of our knowledge, this is the first experimental determination of the indirect bandgap energy at room temperature in h-BN.

From the point view of the momentum conservation, the wave vector of the phonons assisted in the excitation process is the same as that involved in the recombination process, $\boldsymbol{q}=\boldsymbol{MK}$. The dispersion relation of phonons in h-BN[30] indicates that the 85 meV phonon observed here is a longitudinal acoustic (LA) phonon around T-point in the BZ. Therefore, the two lowest energy peaks in the photoexcitation spectrum at 5.93 eV and 6.10 eV can be assigned to the optical excitation between K-point of the VBM to M-point of the CBM assisted by either emitting or absorbing an LA phonon around the T-point with a wave vector $\boldsymbol{q}=\boldsymbol{KM}$ to conserve the momentum and energy. It is worth pointing out that there also appears to be a shoulder near 5.5 eV in the photocurrent excitation spectrum shown in Fig. 2. This band around 5.5 eV has been observed previously in PL emission spectra in high purity HPHT bulk crystals[19,34–36] and in h-BN epilayers grown by a carbon-free CVD method[40] and has been assigned to an indirect exciton transition assisted by multiple phonons.[19] However, the possibility of its origin relating to the presence of impurities such as oxygen cannot be excluded. Our results therefore indicate that the processes of optical excitation crossing the indirect bandgap can take place in h-BN, like the optical recombination processes.[19,36–40]

An energy band diagram near high symmetry K- and M-points in the BZ in h-BN constructed from the photocurrent

excitation spectroscopy (PES) results is shown in Fig. 3, revealing that other than the indirect energy bandgap of $E_g^{MK} = E_g \approx 6.02$ eV (T = 300 K), the minimum direct energy gap is at M-point with $E_g^M = 6.36$ eV (300 K). The next lowest direct energy bandgap is at the K-point with $E_g^K = 6.56$ eV (300 K). The blue arrow line in Fig. 3 illustrates the scenarios of optical excitation between the VBM at K-point and the CBM at M-point via intervalley scattering assisted by LA (T) phonons to achieve the conservation of energy and momentum and so that hυ=E_g±E_p. The band structure also clearly shows that the CBM at K-point is 0.54 eV above that at M-point (i.e., $\Delta E_C^{MK} = 0.54$ eV), while the VBM at K-point is 0.34 eV above that at M-point (i.e., $\Delta E_V^{MK} = 0.34$ eV). The energy difference between the CBM and the VBM at M- and K-points estimated from Fig. 1 of Ref. 18 or from Fig. 3 of Ref. 37 are about 0.5 eV (ΔE_C^{MK}) and 0.3 eV (ΔE_V^{MK}), respectively. The good agreement between the measured and calculated values of ΔE_C^{MK} and ΔE_V^{MK} further affirms our assignments of the observed four peaks near the band-edge in the photoexcitation spectrum shown in Fig. 2.

The identification of the direct minimum energy bandgap bears an important consequence as the optical excitations are more efficient crossing the direct energy bandgap than those crossing the indirect gap involving phonons. The above analysis also provides an improved insight into the band-to-band excitation process with a photon energy of hν. The process can be divided into three energy regions: (a) 5.93 eV < hν < 6.36 eV, electrons are excited into the conduction band at M-point, while holes are generated in the valence band at K-point; this process occurs via scattering by a phonon at T-point with relatively low efficiency, (b) 6.36 eV < hν < 6.56 eV, electrons are excited into the conduction band at M-point while holes are also generated in the valence band at M-point, (c) hν > 6.56 eV, electrons and holes can be excited into their respective bands at K-point. The above understanding is still simplified since valance valley at H-point of the BZ is also very close to K-point.[18,37] Involvement of optical excitation of H-band cannot be excluded but is not considered here.

It is interesting and important to compare the band structures among the III-nitride semiconductors. The conduction bands have a Γ_7 symmetry in both AlN and GaN. In comparison to GaN, the most significant difference in the band structure of AlN is the negative crystal-field splitting Δ_{CF} (−219 meV) compared with a positive value (+38 meV) in GaN.[42,43] Due to this large negative Δ_{CF} in AlN, the order of the valence bands in AlN is different than that in GaN. The top valence band has Γ_9 (Γ_7) symmetry in GaN (AlN) because of the positive (negative) Δ_{cf} Therefore, light emission due to the recombination between the conduction band electrons and the holes in the topmost valence band is polarized with **E⊥c** and **E//c** in GaN and AlN, respectively.[42,43] This fundamental difference has had a large impact in the development of deep UV emitters based on Al-rich AlGaN.[44,53] In sharp contrast, h-BN has a layered crystalline structure and an indirect energy bandgap, the high symmetry points other than the center point in the edges of BZ such as K- and M-points are more important because the CBM and VBM are located at these points. Consequently, impurity energy levels and optical excitation processes involving impurities and bands are expected to be very different in h-BN compared to those in GaN and AlN. For instance, in h-BN, not only the energy levels of impurities, but the positions of wavefunction maxima in the k-space for electrons bound to donors and holes bound to acceptors need to be specified. Otherwise, the properties of impurities are not well defined. While the activation energies of these impurities are measured in the traditional way and optical excitation of an acceptor to the conduction band can be described by hν = E_g^K -E_A, but E_g^K -E_A ≠ E_g - E_A, where $E_g = E_g^{MK}$. The same applies to optical excitation between the valence band and donor, i.e., hν = E_g^M -E_D ≠ E_g - E_D.

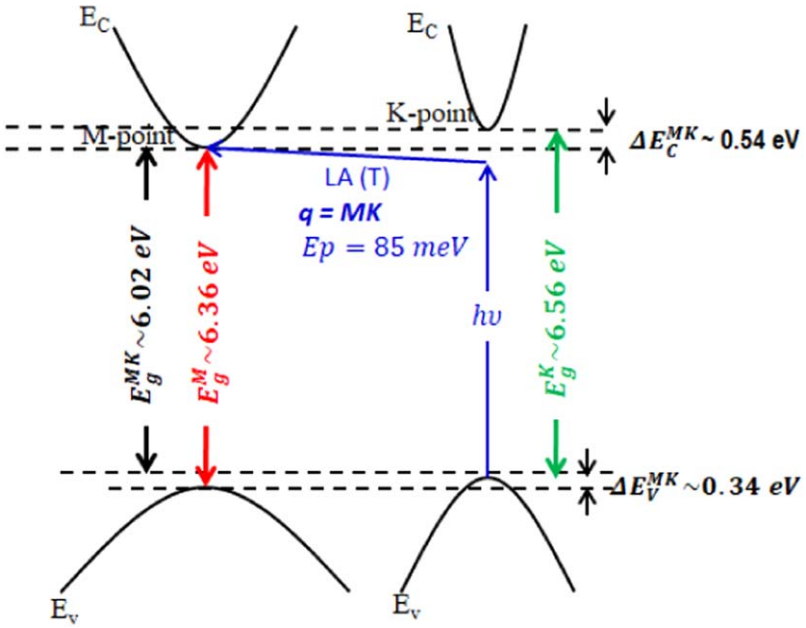

Fig. 3. Room temperature energy band diagram near high symmetry K- and M-points of the BZ in h-BN, constructed from the photocurrent excitation spectroscopy (PES) results, including the indirect energy bandgap of $E_g^{MK} = E_g = 6.02$ eV (black arrow), the minimum direct energy gap at M-point of $E_g^M = 6.36$ eV (red arrow), and the next lowest direct energy bandgap at K-point of $E_g^K = 6.56$ eV (green arrow). Measured energy differences between the CBM and VBM at K- and M-points of ($\Delta E_C^{MK} = 0.54$ eV) and ($\Delta E_V^{MK} = 0.34$ eV) are also indicated and hυ=E_g±E_p.

In summary, h-BN quasi-bulk crystals with a wafer size up to 4-inches in diameter have been produced by HVPE growth technique. The achievement of a pure hexagonal phase and layered structure has been confirmed by XRD, TEM, and Raman characterization results. The layered structure of h-BN introduces some unique features in the band structure, impurity properties, and multi-band involvement in the optical and transport processes. The measured photocurrent excitation spectrum resolved four peaks at the band-edge corresponding to the band-to-band transitions involving the two most relevant high symmetry points of M and K in BZ, from which the room temperature indirect bandgap and minimum direct bandgap energies and the energy differences between the conduction band minima (CBM) and the valence band maxima (VBM) at M- and K-points have been simultaneously determined experimentally for the first time. Our results revealed major differences in the band structures among h-BN and other III-nitrides (InN, GaN, and AlN). Improving understanding of the energy band structures and impurity properties is fundamentally important and a necessary step for the exploration of h-BN for technologically important device applications.

Acknowledgments The information, data, or work presented herein was funded in part by the Advanced Research Projects Agency-Energy (ARPA-E), the U.S. Department of Energy, under Award Numbers DE-AR0001552 and DE-AR0001785 monitored by Dr. Olga Spahn and Dr. Eric Carlson. The views and opinions of the authors expressed herein do not necessarily state or reflect those of the United States Government or any agency thereof. Jiang and Lin are grateful to the AT&T Foundation for the support of Ed Whitacre and Linda Whitacre endowed chairs. The authors would like to thank Dr. Bo Zhao for providing the TEM measurements and analysis.

Author declarations

Conflict of Interest: The authors have no conflicts to disclose.

Data availability

The data that support the findings of this study are available within the article.

ORCID iDs J. Y. Lin https://orcid.org/0000-0003-1705-2635

1) See https://nobelprize.org/prizes/physics/2014/press-release/ for the Nobel Prize in Physics 2014.
2) S. Pimputkar, J. S. Speck, S. P. DenBaars, and S. Nakamura, Nat. Photon **3**, 180 (2009).
3) H. Amano, N. Sawaki, I. Akasaki, and Y. Toyoda, Appl. Phys. Lett. **48**, 353 (1986).
4) S. Nakamura, T. Mukai, and M. Senoh, Appl. Phys. Lett. **64**, 1687 (1994).
5) T. D. Moustakas, U.S. Patent No. 5,686,738.
6) H. X. Jiang and J. Y. Lin, Nat. Electron. **6**, 257 (2023).
7) P. J. Parbrook, B. Corbett, J. Han, T. Y. Seong, and H. Amano, Laser Photonics Rev. **15**, 2000133 (2021).
8) H. Amano et al., J. Phys. D: Appl. Phys. **51**, 163001 (2018).
9) Y. H. Chen, J. Encomendero, C. Savant, V. Protasenko, H. G. Xing, and D. Jena, Appl. Phys. Lett. **124**, 152111 (2024).
10) J. Wu, W. Walukiewicz, K. Yu, J. W. Ager III, E. E. Haller, H. Lu, W. J. Schaff, Y. Saito, and Y. Nanishi, Appl. Phys. Lett. **80**, 4741 (2002).
11) S. Vanka et al., ACS Energy Lett. **5**, 3741 (2020).
12) A. Khan, K. Balakrishnan, and T. Katona, Nature Photon **2**, 77 (2008).
13) A. K. Geim and I. V. Grigorieva, Nature **499**, 419 (2013).
14) R. Bourrellier, S. Meuret, A. Tararan, O. Stephan, M. Kociak, L. H.-G. Tizei, and A. Zobelli, Nano Lett. **16**, 4317 (2016).
15) T. Sugino, K. Tanioka, S. Kawasaki, and J. Shirafuji, Jpn. J. Appl. Phys.Part **236**, L463 (1997).
16) K. Watanabe, T. Taniguchi, and H. Kanda, Nat. Mater. **3**, 404 (2004).
17) Y. Kubota, K. Watanabe, O. Tsuda, and T. Taniguchi, Science **317**, 932 (2007).
18) B. Arnaud, S. Lebe'gue, P. Rabiller, and M. Alouani, Phys. Rev. Lett. **96**, 026402 (2006).
19) G. Cassabois, P. Valvin, and B. Gil, Nat. Photonics **10**, 262 (2016).
20) Y. Hattori, T. Taniguchi, K. Watanabe, and K. Nagashio, Appl. Phys. Lett. **109**, 253111 (2016).
21) C. Yuan, J. Li, L. Lindsay, D. Cherns, J. W. Pomeroy, S. Liu, J. H. Edgar, and M. Kuball, Commun. Phys. **2**, 43 (2019).
22) O. Osberghaus, Zeitschrift fuer Physik **128**, 366 (1950).
23) G. F. Knoll, *Radiation Detection and Measurement* 4th ed. (Wiley, New York, 2010).
24) R. Dahal, J. Li, S. Majety, B. N. Pantha, X. K. Cao, J. Y. Lin, and H. X. Jiang, Appl. Phys. Lett. **98**, 211110 (2011).
25) S. Lu et al., Nat. Commun. **13**, 3109 (2022).
26) A. Maity, S. J. Grenadier, J. Li, J. Y. Lin, and H. X. Jiang, Prog. Quantum Electron. **76**, 100302 (2021).
27) A. Maity, S. J. Grenadier, J. Li, J. Y. Lin, and H. X. Jiang, Appl. Phys. Lett. **116**, 142102 (2020).
28) A. Tingsuwatit, A. Maity, S. J. Grenadier, J. Li, J. Y. Lin, and H. X. Jiang, Appl. Phys. Lett. **120**, 232103 (2022).
29) A. Mballo et al., ACS Omega **7**, 804 (2022).
30) J. Serrano, A. Bosak, R. Arenal, M. Krisch, K. Watanabe, T. Taniguchi, H. Kanda, A. Rubio, and L. Wirtz, Phys. Rev. Lett. **98**, 095503 (2007).
31) L. Wirtz, A. Marini, and A. Rubio, Phys. Rev. Lett. **96**, 126104 (2006).
32) L. Wirtz, A. Marini, M. Gruning, C. Attaccalite, G. Kresse, and A. Rubio, Phys. Rev. Lett. **100**, 189701 (2008).
33) L. Museur and A. Kanaev, J. Appl. Phys. **103**, 103520 (2008).
34) K. Watanabe and T. Tanniguchi, Phys. Rev. B **79**, 193104 (2009).
35) K. Watanabe, T. Taniguchi, T. Kuroda, O. Tsuda, and H. Kanda, Diam. Relat. Mater. **17**, 830 (2008).
36) G. Cassabois, P. Valvin, and B. Gil, Phys. Rev. B **93**, 035207 (2016).
37) L. Artús, M. Feneberg, C. Attaccalite, J. H. Edgar, J. Li, R. Goldhahn, and R. Cuscó, Adv. Photonics Res **2**, 2000101 (2021).
38) T. Q.-P. Vuong, G. Cassabois, P. Valvin, V. Jacques, A. V. D. Lee, A. Zobelli, K. Watanabe, T. Taniguchi, and B. Gil, 2D Mater. **4**, 011004 (2017).
39) V. Alexander, I. Weinstein, and D. Zamyatin, J. Lumines **208**, 363 (2019).
40) S. F. Chichibu, K. Shima, K. Kikuchi, N. Umehara, K. Takiguchi, Y. Ishitani, and K. Hara, Appl. Phys. Lett. **120**, 231904 (2022).
41) S. J. Grenadier, A. Maity, J. Li, J. Y. Lin, and H. X. Jiang, Appl. Phys. Express **15**, 051005 (2022).
42) J. Li, K. B. Nam, M. L. Nakarmi, J. Y. Lin, H. X. Jiang, P. Carrier, and S-H. Wei, Appl. Phys. Lett. **83**, 5163 (2003).
43) G. D. Chen, M. Smith, J. Y. Lin, H. X. Jiang, S.-H. Wei, M. A. Khan, and C. J. Sun, Appl. Phys. Lett. **68**, 2784 (1996).
44) K. B. Nam, J. Li, M. L. Nakarmi, J. Y. Lin, and H. X. Jiang, Appl. Phys. Lett. **84**, 5264 (2004).
45) T. C. Doan, J. Li, J. Y. Lin, and H. X. Jiang, Appl. Phys. Lett. **109**, 122101 (2016).
46) N. D. Zhigadlo, J. Cryst. Growth **402**, 308 (2014).
47) Y. Li, V. Garnier, P. Steyer, C. Journet, and B. Toury, ACS Appl. Nano Mater. **3**, 1508 (2020).
48) Z. Alemoush, N. K. Hossain, A. Tingsuwatit, M. Almohammad, J. Li, J. Y. Lin, and H. X. Jiang, Appl. Phys. Lett. **122**, 012105 (2023).
49) Z. Alemoush, A. Tingsuwatit, A. Maity, J. Li, J. Y. Lin, and H. X. Jiang, J. Appl. Phys. **135**, 175704 (2024).
50) L. Weston, D. Wickramaratne, M. Mackoit, A. Alkauskas, and C. G. Van de Walle, Phys. Rev. B **97**, 214104 (2018).
51) F. Oba, A. Togo, I. Tanaka, K. Watanabe, and T. Taniguchi, Phys. Rev. B **81**, 075125 (2010).
52) M. Almohammad, Z. Alemoush, J. Li, J. Y. Lin, and H. X. Jiang, Appl. Phys. Lett. **124**, 102106 (2024).
53) Z. Zhang, M. Kushimoto, T. Sakai, N. Sugiyama, L. J. Schowalter, C. Sasaoka, and H. Amano, Appl. Phys. Express **12**, 124003 (2019).